Proc. Indian Acad. Sci. (*Chem. Sci.*), Vol. 113, Nos 5 & 6, October–December 2001, pp 527–537

AC impedance behaviour and state-of-charge dependence of $Zr_{0\cdot5}Ti_{0\cdot5}V_{0\cdot6}Cr_{0\cdot2}Ni_{1\cdot2}$ metal-hydride electrodes

S RODRIGUES[a], N MUNICHANDRAIAH[b]* and A K SHUKLA[a]*
[a]Solid State and Structural Chemistry Unit, and
[b]Department of Inorganic and Physical Chemistry, Indian Institute of Science, Bangalore 560 012, India
e-mail: muni@ipc.iisc.ernet.in; shukla@sscu.iisc.ernet.in

Abstract. Metal-hydride electrodes made of an AB_2 alloy of the composition $Zr_{0\cdot5}Ti_{0\cdot5}V_{0\cdot6}Cr_{0\cdot2}Ni_{1\cdot2}$ are studied for AC impedance behaviour at several of their state-of-charge values. Impedance data at any state-of-charge comprise two RC-time constants and accordingly are analysed by using a nonlinear-least-square-fitting procedure. Resistance of the electrode and frequency maximum (f*) of the low-frequency semicircle are found useful for predicting state-of-charge of the metal-hydride electrodes.

Keywords. Hydrogen-storage alloy; metal-hydride electrode; AC impedance; AB_2 alloys; state-of-charge.

1. Introduction

The ratio of available capacity of a cell to its maximum attainable capacity is referred to as its state-of-charge (SOC). An estimation of SOC of the electrodes facilitates their optimum utilization for a given application as well as an evaluation of their state-of-health. AC impedance measurements provide knowledge of several parameters, the magnitudes of which may depend on the SOC of the cell[1–4]. AC impedance measurements involve excitation of the electrochemical cell by an AC voltage of small amplitude (~5 mV) and evaluation of the resistive and reactive components as well as other related parameters such as modulus of impedance and phase angle. As the measurement encompasses a wide range of AC signal frequencies, various characteristic parameters of the electrochemical cell and kinetics of the associated reactions can be evaluated.

Metal-hydride (MH) electrodes form the anode or the negative plate of a nickel-metal-hydride battery. However, the development of MH electrode materials, which yield high energy per unit weight with a long charge/discharge cycle life, has been quite challenging. To this end, several AB_2 and AB_5-type alloys have been investigated[5]. Although AB_5-type alloys were preferred in the past, presently the preference is for AB_2-type alloys[6]. When a MH electrode in an alkaline electrolyte (usually 6 M KOH) is subjected to charging, reduction of H_2O molecule takes place producing atomic hydrogen on its surface in adsorbed state. Penetration of adsorbed hydrogen into the bulk of the electrode material results in the formation of MH alloy which behaves as a reservoir of hydrogen in the battery.

*For correspondence

In this communication, we report the impedance behaviour of MH electrodes made of $Zr_{0·5}Ti_{0·5}V_{0·6}Cr_{0·2}Ni_{1·2}$ alloy and have analysed the data for predicting SOC of the electrodes.

2. Experimental

An AB_2-type alloy of the composition $Zr_{0·5}Ti_{0·5}V_{0·6}Cr_{0·2}Ni_{1·2}$ has been recently investigated for rechargeable Ni-MH and Ag-MH batteries [7–9]. In order to prepare the metal-hydride electrodes, the ingot of $Zr_{0·5}Ti_{0·5}V_{0·6}Cr_{0·2}Ni_{1·2}$ alloy was pulverized mechanically and was passed through graded sieves to obtain alloy particles in the range 50–73 μm (average particle-size: 60 μm). Roll-compacted metal-hydride electrodes were then prepared by mixing the alloy powder (85 wt.%), graphite (10 wt.%) and poly-tetra fluoroethylene (PTFE GP2-Fluon) suspension (5 wt.%). The resulting paste was spread as a thin layer onto a degreased nickel mesh (4 cm × 3 cm) and compacted at a pressure of 3000 kg cm^{-2} for 5 min followed by heat treatment in hydrogen atmosphere at 350°C for 30 min.

A cell was assembled in a polypropylene container by inserting the MH electrode symmetrically between two large nickel electrodes in 6 M KOH electrolyte under flooded condition. A Hg/HgO, OH^- (6 M) reference electrode (MMO) was used. The electrode was subjected to about 10 charge/discharge cycles by using a galvanostatic electrical circuit. During the course of these cycles, the activation of the MH electrode took place and the discharge capacity of about 320 mAh g^{-1} of the MH alloy was obtained at a cut-off potential of –0·93 V vs MMO. Subsequent to activation, the MH electrode was subjected to AC impedance measurements using the reference electrode at its several SOC values. For this purpose, the electrode was charged to about 10% excess of its discharge capacity and allowed to rest for about 2 h before recording the impedance spectrum at SOC~1. The electrode was discharged at C/10 rate to a predetermined value of SOC, and it was allowed to equilibrate for about 2 h prior to the impedance measurements. This procedure was followed for several values of SOC values of the electrode between 0 and 1.

3. Results and discussion

During discharge of a MH electrode in an alkaline electrolyte the following reaction steps occur:

$$MH_{abs} \rightarrow MH_s, \tag{1}$$

$$MH_s + OH^- \rightarrow M + H_2O + e^-. \tag{2}$$

Equation (1) represents transport of hydrogen from bulk of the alloy powder (MH_{abs}) to its surface by diffusion, i.e. change from the absorbed state to the adsorbed state. The surface hydrogen (MH_s) at the electrode/electrolyte interface can undergo electrochemical oxidation as shown in reaction (2). In the completely discharged state, the MH electrode reaches nearly a pure state of the alloy composition (M) whereas in its fully-charged state, the electrode possesses maximum absorbable atomic hydrogen. The nature of the electrode varies between these two extremes as the state-of-charge changes from 0 to 1. The variation of steady value of the open-circuit potential (E) of the MH electrode

with SOC is shown in figure 1. The value changes from –0·927 V vs MMO at SOC~1 to about –0·82 V vs MMO at SOC~0·1 with a fair degree of linearity. Since the MH electrode behaves as a reversible electrode, the variation on E may be explained on the basis of the Nernst equation. Under open-circuit condition, (1) and (2) are considered equilibrium processes and are rewritten as in (3) and (4), respectively.

$$MH_{abs} \quad MH_s, \tag{3}$$

$$MH_s + OH^- \quad M + H_2O + e^- . \tag{4}$$

Equation (3) represents equilibrium between absorbed hydrogen and surface hydrogen. The quantity of available hydrogen is thus the deciding factor for SOC of the electrodes. Equation (4) is the potential-determining step and the potential (E) of the MH electrode is defined by the Nernst equation as,

$$E = E^0 - (2{\cdot}303RT/F)\log_{10}(C_H.C_{OH^-}), \tag{5}$$

where E^0 is the standard electrode potential, C_H is the concentration of available hydrogen at the MH electrode, and C_{OH^-} is the concentration of alkali in the electrolyte. Since SOC is the ratio of available capacity to the maximum attainable capacity, it may be expressed as,

$$SOC = C_H/C^0_H, \tag{6}$$

where C^0_H is the saturation concentration of hydrogen at the MH electrode at SOC~1. Accordingly, (5) may be written as,

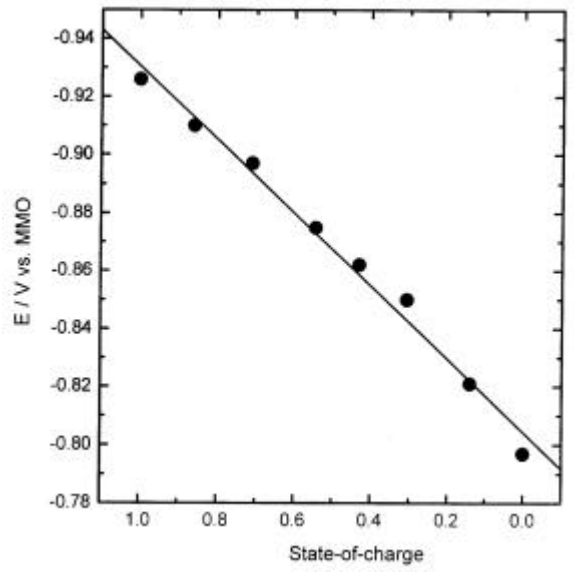

Figure 1. Variation of metal-hydride electrode potential (E) with state-of-charge.

$$E = E^0 - 2{\cdot}303RT/F \log_{10}(\mathrm{SOC}).C^{\circ}{}_{\mathrm{H}}.C_{\mathrm{OH}^-}. \quad (7)$$

Since $C^0{}_{\mathrm{H}}$ and C_{OH^-} are constants, (7) may thus be reduced to,

$$E = K - 0{\cdot}06 \log_{10}(\mathrm{SOC}), \quad (8)$$

where K is a constant. On differentiation, (8) becomes,

$$\mathrm{d}E/\mathrm{d}\log_{10}(\mathrm{SOC}) = -0{\cdot}06 \text{ V}. \quad (9)$$

Equation (9) predicts the variation of about 60 mV when the SOC of the MH electrode change from 1 to 0·1. The value of the potential variation, obtained from figure 1, however, is about 120 mV instead of 60 mV. It thus seems that the potential-determining step of the MH electrode reaction is not as simple as it is shown in (4). Since the experimental value of 120 mV is twice the theoretical value of 60 mV, it appears that E and SOC are related as,

$$E = K - 0{\cdot}06 \log_{10}(\mathrm{SOC})^2, \quad (10)$$

and not by (8). Therefore, the value of (dE/dlog (SOC)) becomes 120 mV. In order to satisfy (10), the appropriate potential-determining electron-transfer step appears to have a complex nature.

For predicting the SOC of MH electrodes, the open-circuit electrode potential may be useful. The AC impedance spectra recorded at several SOC values of the MH electrode are shown as Nyquist and Bode plots in figures 2 and 3, respectively. At any SOC value, the impedance spectrum is characterized by two RC-time constants. In the Nyquist plot (figure 2), the high-frequency semicircle due to the geometry of the MH electrodes is more clearly noticeable than for the case of alloy ingot electrode. Thus the low-frequency semicircle is attributed to parallel arrangement of charge-transfer resistance (R_{ct}) of reaction (4) and double-layer capacitance (C_{dl}) of the MH electrode/electrolyte interface. Accordingly, the impedance data were subjected to non-linear least-square (NLLS)-fitting[10] using an equivalent-circuit shown in figure 4. The circuit-description code (CDC) employed for fitting the data is $R_\Omega(R_1Q_1)(R_{\mathrm{ct}}Q_2)$, where R_Ω stands for solution resistance, R_1 and Q_1 respectively stand for geometric electrode resistance and constant phase element corresponding to the high-frequency semi-circle, and Q_2 for the constant phase element corresponding to the low-frequency semi-circle. Since the data show overlap of RC-time constant, constant phase elements (Q_1 and Q_2) were employed in place of capacitive elements. All impedance data are found to fit the equivalent-circuit and the typical correlation factors are given in table 1. A low value of (c^2) and a value of at least ± 0·1 for correlation coefficient of a majority of the impedance parameters ensure confidence in the values of the impedance parameters[11,12]. The theoretical data generated from the fit results are shown as solid lines in figures 2 and 3 in Nyquist and Bode forms, respectively, and the fit values are given in table 2. It is seen that the theoretical data agree well with the experimental data (figures 2 and 3). The variation in resistive components of the impedance with SOC of the electrode is shown in figure 5. The value of R_Ω is nearly invariant at about 1 Ω. The discharge reaction of the MH electrode (reaction 2) suggests that the electrolyte gets diluted with a decrease in SOC of the electrode, and therefore a variation in the electrolyte resistance with SOC may be

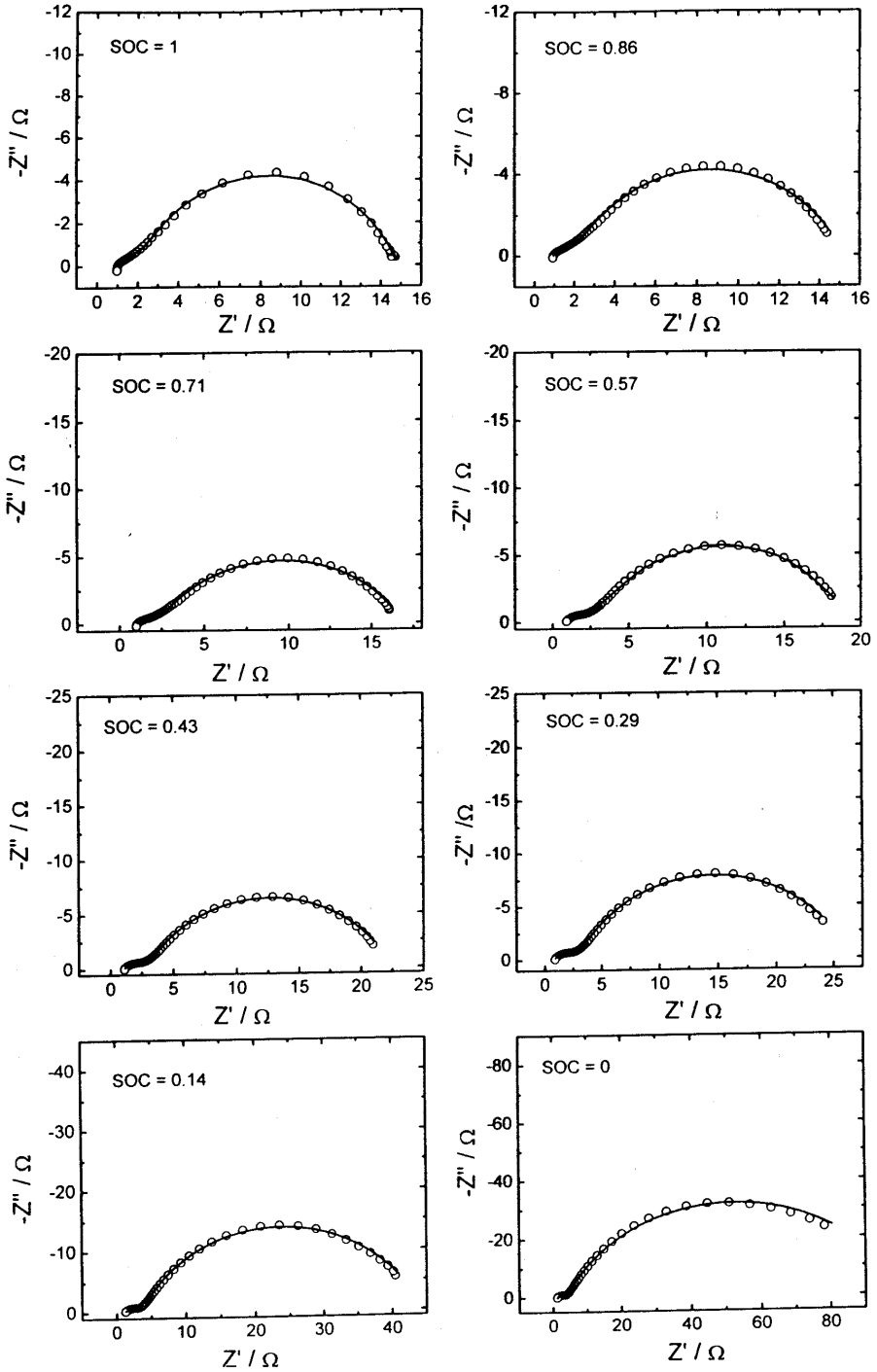

Figure 2. Electrochemical impedance spectra in Nyquist form of metal-hydride electrode. The experimental data are shown as symbols and theoretical data obtained from NLLS-fit results are shown as solid curves.

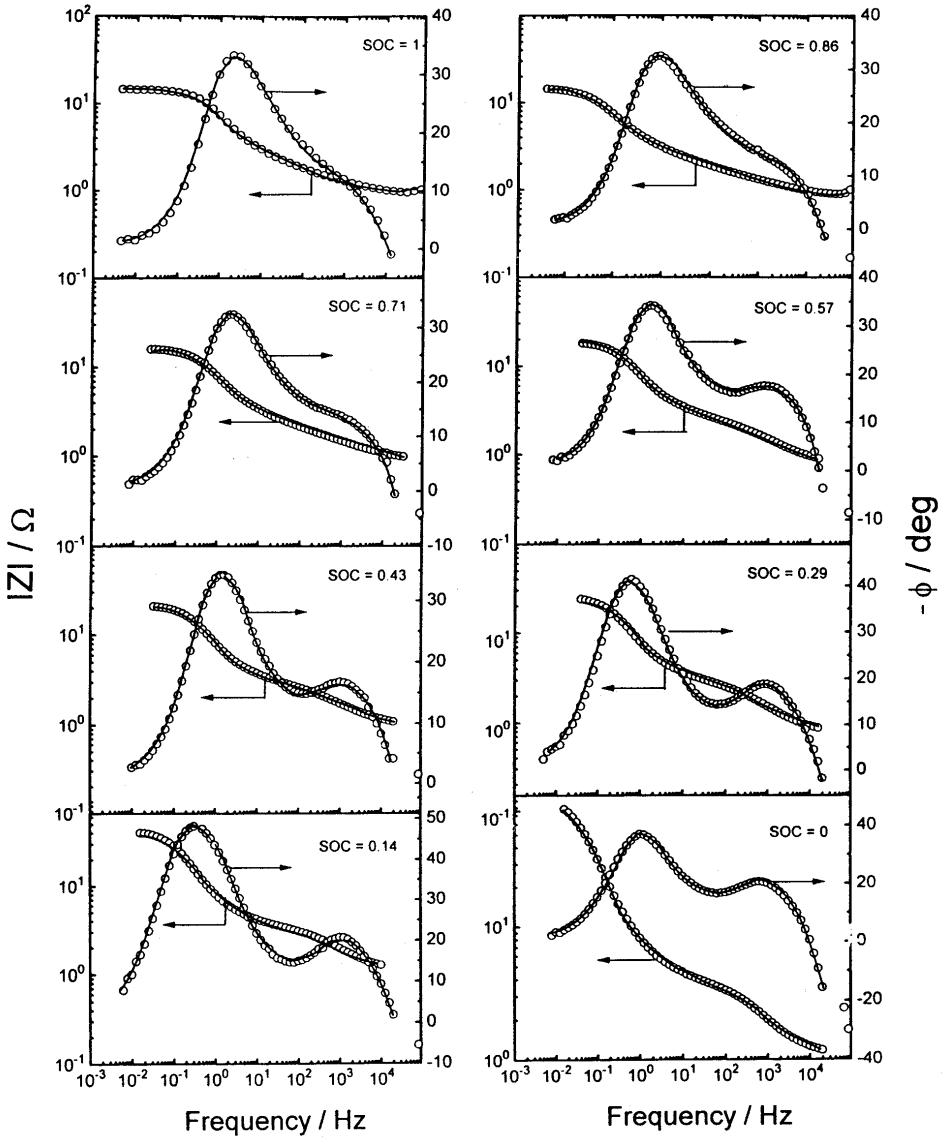

Figure 3. Electrochemical impedance spectra in Bode form of metal-hydride electrode. The experimental data are shown as symbols and theoretical data obtained from NLLS-fit results are shown as solid curves.

expected. On the contrary, the value of R_Ω is nearly constant (figure 5a) perhaps due to a large excess of concentrated electrolyte (6 M KOH) in the cell. The value of R_1 is 1·2 Ω at SOC~1, and it increases linearly with a decrease in SOC reaching a value of about 2·8 Ω at SOC~0·1 (figure 5b). During repeated charge/discharge cycling, the MH alloy particles undergo volumetric deformation due to absorption/desorption of hydrogen. As a result, a large number of micro-cracks develop on the alloy particles as seen under a scanning electron microscope[13]. It is therefore probable that the particles possess

Table 1. Correlation factors of NLLS-fit parameters for electrochemical impedance data of the metal-hydride electrode at SOC~0. $\chi^2 = 8{\cdot}6 \times 10^{-4}$.

Parameters	R_Ω	R_1	Q_1	n_1	R_{ct}	Q_2	n_2
R_Ω	1·00						
R_1	0·54	1·00					
Q_1	−0·58	−0·79	1·00				
n_1	0·66	0·79	−0·99	1·00			
R_{ct}	−0·17	−0·55	0·35	−0·34	1·00		
Q_2	0·01	0·21	−0·04	0·05	−0·57	1·00	
n_2	−0·21	−0·73	0·44	−0·43	0·72	−0·69	1·00

Table 2. Impedance parameters at different SOC values of the metal-hydride electrode.

SOC	0	0·14	0·29	0·43	0·57	0·71	0·86	1·00
Voltage (V)	−0·80	−0·82	−0·85	−0·86	−0·88	−0·90	−0·91	−0·93
R_Ω (Ω)	0·99	0·93	1·00	0·81	1·03	0·81	1·07	1·14
R_1 (Ω)	1·24	1·19	1·58	2·00	2·09	2·21	2·66	2·64
$10^{-3}Q_1$ (Ω^{-1})	9·35	5·59	8·11	5·78	4·07	2·97	3·47	1·22
n_1	0·64	0·67	0·59	0·58	0·61	0·65	0·60	0·73
R_{ct} (Ω)	12·62	13·00	14·23	16·54	19·25	23·4	40·5	97·4
$10^{-2}Q_2$ (Ω^{-1})	2·49	2·54	2·40	2·58	2·50	2·54	2·57	2·64
n_2	0·75	0·72	0·74	0·75	0·75	0·75	0·76	0·74

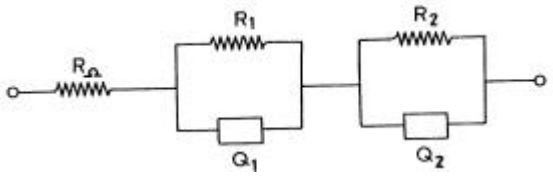

Figure 4. Equivalent circuit used for NLLS-fit. R_Ω, R_1 and R_2 refer to ohmic resistance, resistance corresponding to the high frequency semicircle and charge-transfer resistance respectively. Q_1 and Q_2 refer to constant phase elements corresponding to capacitance of the high frequency semicircle and double-layer capacitance respectively.

increased voids with a decrease in SOC due to consumption of absorbed hydrogen by the discharge reaction (reaction 2). This may result in an increased resistance of the alloy as reflected in an increase in the magnitude of R_1 with a decrease in SOC. Since the increase of R_1 is linear (figure 5b), it is perhaps a useful parameter for prediction of SOC of the MH electrode. There is a gradual increase in the magnitude of R_{ct} (figure 5c) from about 13 Ω at SOC~1 to about 23 Ω at SOC~0·3, due to a decrease in concentration of available hydrogen as SOC of the electrode decreases. However, there is a sudden increase in the

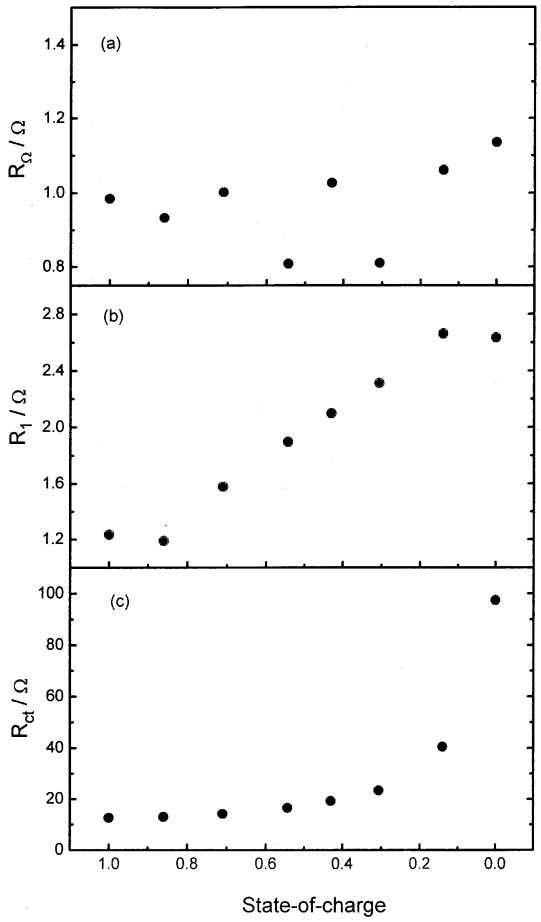

Figure 5. Variation of resistive components of impedance with state-of-charge. Area of the electrode = 2 cm^2 and mass of alloy powder = 0·1 g.

magnitude of R_{ct} at the SOC values close to 0 (figure 5c). Although the variation is non-linear between SOC values of 1 and 0, R_{ct} is also a useful parameter for prediction of SOC of the MH electrode. There is no regular trend of variation in the case of constant phase elements (Q and n) and therefore these parameters do not appear to be important for prediction of SOC of the MH electrode.

A comparison of impedance spectra of different SOC values (figure 2) indicates that the low-frequency semicircle part of the spectrum grows in size with a decrease in SOC of the electrode. It is therefore considered that the frequency (f*) corresponding to the maximum value of $-Z''$ of the semicircle as well as Z' and Z'' may show dependence on SOC. Accordingly, the variation of f*, Z' and Z'' are shown in figures 6 and 7. The value of f* is about 700 mHz at SOC~1 and decreases linearly to about 50 mHz at SOC~0, and therefore f* is useful for prediction of SOC (figure 6). On the other hand, Z' and Z'' do not show any useful variation for this purpose (figure 7). Since C_s and R_s were examined

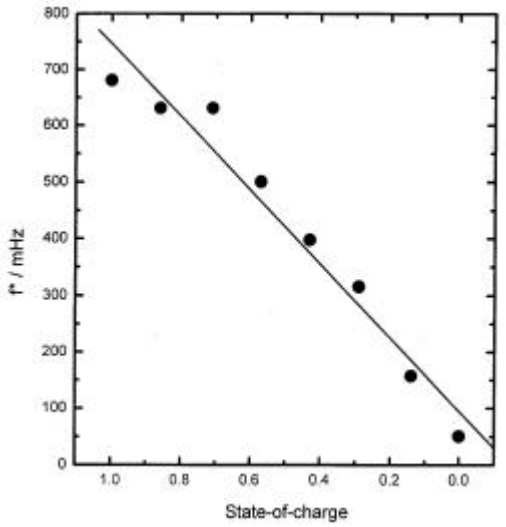

Figure 6. Variation of frequency maximum (f^*) with state-of-charge of a metal-hydride electrode.

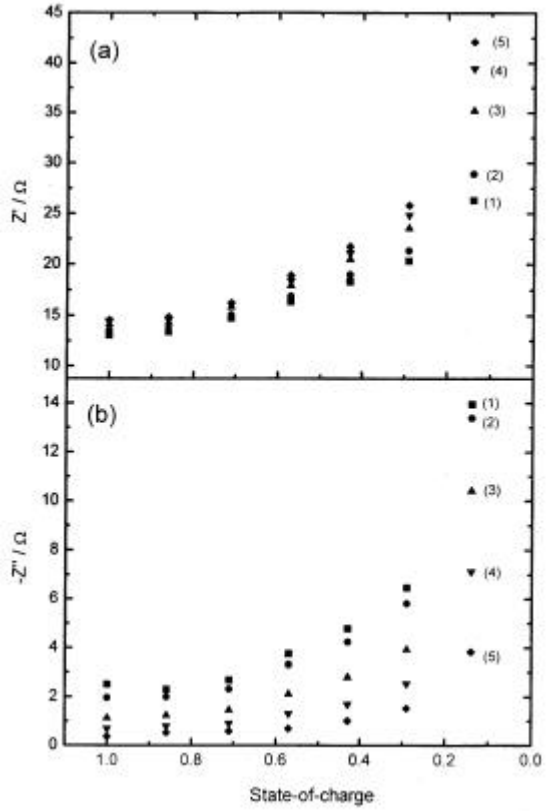

Figure 7. Variation of (**a**) Z' and (**b**) Z'' with state-of-charge of a metal-hydride electrode at 10 (1), 25 (2), 50 (3), 100 (4) and 125 mHz (5).

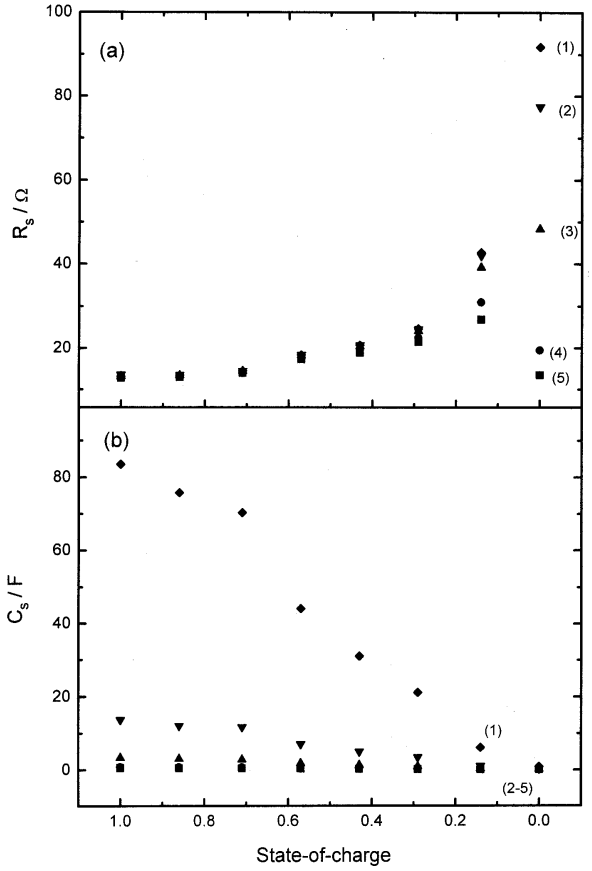

Figure 8. Variation of (**a**) equivalent series resistance (R_s) and (**b**) equivalent series capacitance (C_s) with state-of-charge of a metal-hydride electrode at 10 (1), 25 (2), 50 (3), 100 (4) and 125 mHz (5).

for SOC prediction of several battery systems, these parameters are calculated using the following equations for the MH electrode at several frequency values.

$$C_s = C_{dl}\,[1 + 1/(\omega R_{ct} C_{dl})^2], \tag{11}$$

$$R_s = R_{ct}/[1+(\omega R_{ct} C_{dl})^2]. \tag{12}$$

In (11) and (12), R_s is the equivalent series resistance and C_s is the equivalent series capacitance. C_{dl} $(= 1/(2\pi f^* R_{ct}))$ can be obtained from the maximum frequency corresponding to the maximum on the semi-circle (f^*) and R_{ct} corresponds to the low-frequency intercept on the real axis. For this purpose, Q_2 is assumed to be equal to C_{dl}. It is also found that C_{dl} values calculated from f^* and diameter of the low-frequency semicircle are nearly the same as Q_2 values obtained from the fitting procedure. The variation of C_s and R_s is shown in figure 8 as a function of SOC of the MH electrodes. It

may be seen that C_s values calculated at very low frequencies show a linear variation with SOC of the MH electrodes.

4. Conclusions

MH electrodes made of AB_2 alloy of the composition $Zr_{0·5}Ti_{0·5}V_{0·6}Cr_{0·2}Ni_{1·2}$ are studied for AC impedance behaviour at several SOC values. The impedance data at any SOC value comprises two RC-time constants and accordingly the data are analysed using NLLS-fitting procedure. The resistance (R_1) of the electrode and frequency maximum (f^*) of the low-frequency semicircle are found useful for predicting SOC of the MH electrodes.

References

1. Willinhnganz E 1941 *Trans. Am. Electrochem. Soc.* **79** 253
2. Hampson N A, Karunathilaka S A G R and Leek R 1980 *J. Appl. Electrochem.* **10** 3
3. Huet F 1998 *J. Power Sources* **70** 59
4. Rodrigues S, Munichandraiah N and Shukla A K 2000 *J. Power Sources* **87** 12
5. Appleby A J, Kita H, Chemla M and Bronoel G 1973 *Encyclopedia of electrochemistry of the elements* (ed.) A J Bard (New York: Marcel Dekker) vol 9, p. 384
6. Ganesh Kumar V 1999 *Studies on nickel/metal-hydride, lithium-ion and valve-regulated lead/acid batteries*, Ph D thesis, Indian Institute of Science, Bangalore, p. 75
7. Ganesh Kumar V, Shaju K M, Munichandraiah N and Shukla A K 1998 *J. Power Sources* **76** 106
8. Ganesh Kumar V, Shaju K M, Munichandraiah N and Shukla A K 1999 *J. Solid State Electrochem.* **3** 470
9. Rodrigues S, Munichandraiah N and Shukla A K 1999 *J. Appl. Electrochem.* **29** 1285
10. Boukamp B A 1989 *Equivalent Circuit*, Users Manual, University of Twente, Enschede, The Netherlands
11. Alt A 1990 *Exploring hyperspace – A non mathematical explanation of multivariate analysis* (London: McGraw-Hill)
12. Bevington R R 1969 *Data reduction and error analysis for the physical sciences* (New York: McGraw Hill)
13. Ganesh Kumar V, Shaju K M, Rodrigues S, Munichandraiah N and Shukla A K 2000 *J. Appl. Electrochem.* **30** 349